REPORT DOCUMENTATION PAGE

Form Approved
OMB NO. 0704-0188

1. AGENCY USE ONLY *(Leave blank)*	2. REPORT DATE	3. REPORT TYPE AND DATES COVERED
		~~Reprint~~

4. TITLE AND SUBTITLE

TITLE ON ~~REPRINT~~

5. FUNDING NUMBERS

DAAG55-98-1-0277

6. AUTHOR(S)

AUTHOR(S) ON ~~REPRINT~~

7. PERFORMING ORGANIZATION NAMES(S) AND ADDRESS(ES)

Boise State University

8. PERFORMING ORGANIZATION REPORT NUMBER

9. SPONSORING / MONITORING AGENCY NAME(S) AND ADDRESS(ES)

U.S. Army Research Office
P.O. Box 12211
Research Triangle Park, NC 27709-2211

10. SPONSORING / MONITORING AGENCY REPORT NUMBER

ARO 37739.1-EV-DPS

11. SUPPLEMENTARY NOTES

The views, opinions and/or findings contained in this report are those of the author(s) and should not be construed as an official Department of the Army position, policy or decision, unless so designated by other documentation.

12a. DISTRIBUTION / AVAILABILITY STATEMENT

Approved for public release; distribution unlimited.

12 b. DISTRIBUTION CODE

13. ABSTRACT *(Maximum 200 words)*

ABSTRACT ON ~~REPRINT~~

20011113 163

14. SUBJECT TERMS			15. NUMBER IF PAGES
			16. PRICE CODE
17. SECURITY CLASSIFICATION OR REPORT	18. SECURITY CLASSIFICATION OF THIS PAGE	19. SECURITY CLASSIFICATION OF ABSTRACT	20. LIMITATION OF ABSTRACT
UNCLASSIFIED	UNCLASSIFIED	UNCLASSIFIED	UL

TOMOGRAPHIC INVERSION OF CROSSHOLE RADAR DATA: CONFIDENCE IN RESULTS

William P. Clement and Michael D. Knoll
Center for the Geophysical Investigation of the Shallow Subsurface
1910 University Drive
Boise State University
Boise, ID 83725

ABSTRACT

Crosshole radar tomography is increasingly being used to characterize the shallow subsurface and to monitor hydrologic processes. Although tomographic inversion provides a subsurface model, confidently interpreting the resulting image can be challenging. We conducted a simple modeling study to better understand the capabilities and limitations of tomographic inversion. We start with a known earth model, simulate a tomography experiment, and invert the synthetic data. We investigate the effects of straight and curved ray approximations to wave propagation, regularization, grid size, and starting model. We also investigate the effects of limited ray coverage through the earth model and noise in the data. Understanding the effects of these different methods and parameterizations will help us place confidence limits on modeled features to more accurately reflect our knowledge of the subsurface.

INTRODUCTION

Crosshole radar tomography is increasingly being used to characterize the shallow subsurface and to monitor hydrologic processes such as infiltration through the vadose zone and solute transport through the saturated zone. While collecting, processing, and inverting radar tomography data is not difficult, interpreting the resulting images with confidence can be a challenge. Are parameter estimates accurate, or are they artifacts of the inversion process? What constraints should be used in the inversion process to improve results? Methods to determine the quantitative resolution, uncertainty, and reliability of tomographic images are greatly needed.

As a first step towards addressing these issues, we conducted a simple modeling study. We start with a known earth model, simulate a tomography experiment, and invert the synthetic data. By comparing the inversion results with the starting model, we can improve our understanding of the capabilities and limitations of different tomographic inversion methods.

We used two different inversion algorithms: one straight ray and one curved ray. We also investigated the effects of including different types of constraints in the inversion, as well as the effects of ray coverage, uncertainty in traveltime picks, model discretization, and starting model. Good references on tomography and inverse theory include Menke (1989) and Snieder and Trampert (1999).

The earth model that we selected is representative of the types of features and electrical property variations that we expect at the Boise Hydrogeophysical Research Site (BHRS), the focus of an intense investigation of geophysical and hydrologic parameter distribution in a heterogeneous, coarse, alluvial aquifer (Barrash et al., 1999; Clement et al., 1999; Peterson et al., 1999). The synthetic modeling results in this paper provide insight into the capabilities and limitations of different tomography methods and the level of detail that can be reliably interpreted from tomographic images of the site.

BACKGROUND THEORY

Matrix algebra provides a convenient way to express forward and inverse modeling problems such as travel time tomography. The forward problem is:

$$Gm = d,$$

where d is the data (vector), G is the kernel function (matrix), and m is the model (vector). The data are the projection of the model by the kernel function. The kernel function represents the physics of the problem, including boundary conditions and differential equations.

A solution to the inverse problem is:

$$m = G^{-1}d.$$

The inversion process involves computing the inverse of matrix G and then multiplying this matrix by the data to compute the model. Unfortunately, G^{-1} can be difficult to compute, particularly if the matrix is ill-conditioned (small data errors cause large model changes), ill-posed (mix-determined) (Snieder and Trampert, 1999), or large (too many parameters for available computer memory). In these cases, a weighted, damped, least squares approach is often used to find a solution (Menke, 1989):

$$m^{est} = \langle m \rangle + [G^T W_e G + \lambda^2 W_m]^{-1} G^T W_e [d - G\langle m \rangle]$$

where m^{est} is the best fitting model, $\langle m \rangle$ is the starting model, d and G are the data and the kernel as before, W_m is the regularization or model weighting matrix, W_e is the data weighting matrix, and λ is the weighting factor between prediction error (overdetermined) and solution length (underdetermined). The parameter λ determines how much the data influences the model versus how much the model is constrained by the regularization. For $\lambda = 0$, the solution depends only on the data. For large λ values, the solution depends more on the regularization.

The least squares approach minimizes the L2 norm to determine the optimal solution, i. e.,

$$\text{Min}\left(\sqrt{\left(\sum_i |e_i|^2\right)}\right)$$

where e_i are the differences between the observed and calculated data. In the tomography problem, the data are first arrival times and we try to minimize the difference between the calculated and observed times.

Tomographic data sets often consist of many measurements. The result is that matrices can be large, sparse, and difficult to invert directly. A variety of computational methods have been developed to implement matrix inversions, including ART (e. g., Peterson et al, 1985), SIRT (e. g., Tweeton, 1988), and LSQR (Paige and Saunders, 1982), which are all iterative solvers. We use a straight ray tomographic inversion using SIRT (Tweeton, 1988) and a curved ray inversion using LSQR (Aldridge and Oldenburg, 1993).

FORWARD MODELING

To test different crosshole traveltime tomography algorithms, we used a finite-difference approximation to the eikonal equation (Vidale, 1990) to simulate a crosshole radar tomography experiment. The eikonal equation calculates the first arrival travel time of a propagating wave through a gridded velocity field. Figure 1 shows the input velocity model. The model is 5 m by 10 m with a horizontal and vertical grid spacing of 0.05 m. We included several layers, some with lateral velocity changes, to simulate features that we believe exist at the BHRS. The input velocity model consists of high and low velocity zones and thick and thin layers to test the inversion

schemes. The upper, layer, 2 m thick, represents the vadose zone with a velocity of 0.140 m/ns. Velocities in the saturated zone (2 - 10 m depth) range from 0.070 to 0.095 m/ns. Layers are horizontal and range in thickness from 0.5 to 2.0 m. The layer at 4.0 to 5.5 m depth includes a low velocity inclusion in the center of the model, between 2.0 and 3.5 m on the horizontal scale; at the edges of the model, the velocity is 0.090 m/ns while in the center the velocity is 0.070 m/ns. Another lateral velocity change is included in the layer between 7.0 and 8.0 m depth. Close to the wells, the velocity is 0.080 m/ns while in the center, between 2.0 and 3.5 m on the horizontal scale, the velocity is 0.090 m/ns. These horizontal velocity changes are included to determine the ability of the inversion methods to image heterogeneity in the subsurface.

We simulated a traveltime tomography experiment in two wells spaced 3.5 m apart. Travel times were computed between 40 shot locations (0.25 m vertical spacing) and 41 receiver locations (also 0.25 m vertical spacing).

We used two forward modeling algorithms to invert the synthetic crosshole traveltime data. The first algorithm uses the same forward model scheme as was used to generate the synthetic data (Aldridge and Oldenburg, 1993). This algorithm can simulate ray-bending at velocity contrasts. We also used a straight-ray forward modeling algorithm for comparison (Tweeton, 1988). In both cases, the simulated tomographic data consists of 1640 first arrival times.

RESULTS OF INVERSION

Straight Ray versus Curved Ray Simulators

Figure 1 shows the input model and a comparison of the straight ray and curved ray inversions using noise-free data. Velocity values were determined on a 0.1 m grid, and then upscaled to 0.25 m for display. The straight ray inversion smooths the velocity in each pixel using an average of its near neighbors to compensate for the fine grid spacing. The curved ray method uses regularization to condition the problem; in this simulation, we used a flatness constraint with 10:1 horizontal to vertical regularization.

Results show that the curved ray simulator is better able to locate boundaries than the straight ray simulator. The curved ray model has a sharp velocity change from about 0.140 m/ns in the upper 2 m to velocities less than 0.100 m/ns in the lower 8 m of the model. This boundary is smeared in the straight ray model. Both models also provide a hint of the alternating high and low velocities with depth. Again, the boundaries are more distinct in the curved ray model. The models also show lateral velocity changes in the center of the domain, although the boundaries of the inclusions are not particularly well resolved.

How do the two inversion solutions compare to the true velocity field? The straight ray model has a velocity range of 0.059 to 0.150 m/ns, somewhat greater than the true range, with an average misfit error of 0.005 ns and an RMS misfit error of 0.102 ns. The range of error values for the straight ray model is -0.509 to 0.539 ns. The curved ray model has a velocity range of 0.069 to 0.157 m/ns, an average misfit error of -0.012 ns, and an RMS error of 0.239 ns. The misfit range for the curved ray model is -0.863 to 1.836 ns. Both methods have an average error near zero, but the curved ray method has a larger RMS error indicating a larger variance in the misfit error.

To gain insight into how the two inversion methods partition error along ray paths, we generated plot of ray density for both methods. Ray density is defined as the total raypath length per slowness cell divided by the grid interval. Figure 2 show the ray density of the two inversion methods. For the straight ray inversion, more rays pass through the center of the model than at the edges. The ray coverage decreases systematically away from the model's center. This coverage difference will cause the inversion algorithm to assign errors to the less densely sampled cells

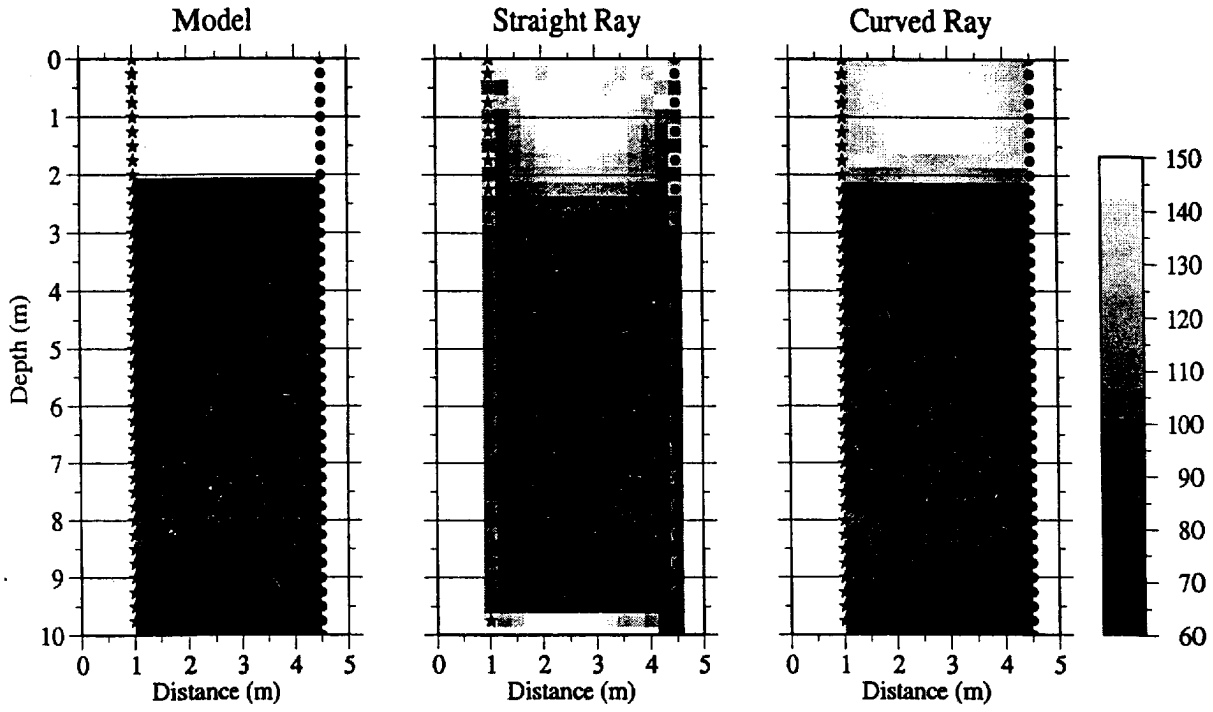

Figure 1. Velocity models from straight and curved ray inversion methods. The true model is on the left. The inverted model from the straight ray inversion method is in the center and the curved ray inversion model is on the right. The grayscale indicates velocities in m/ms. The stars are sources and the circles are receivers. White spots in the figures above 2 m are where velocities are greater than 150 m/ms, or where rays do not sample the grid, as along the bottom of the straight ray model.

because they affect less of the travel times. Thus, the edges of the model are less constrained than the middle and, consequently, our uncertainty is greater for the edges. From the ray coverage, we have more confidence in the modeled features in the region between 3 to 7 m depth and 1.5 to 4 m distance.

The curved ray inversion has a much different ray coverage character. Thin zones of higher coverage exist in the model. High ray density zones extend horizontally, most notably at 1.5 to 2.0 m. Another strong horizontal band is between 8.5 to 9 m. These bands correspond to the high velocity zones in the input model. Diagonal zones of high ray density also exist in the ray coverage. As in the straight ray case, the edges of the model are sampled by fewer rays. Again, our confidence in the middle portion of the model is higher.

Noting the ray coverage, we would still have confidence in the models' layering, but we would be less certain of the lateral velocity changes, especially at the model boundaries. We could improve the ray coverage at the edges by increasing our cell size, thus including more data per cell. However, we must have a sufficiently fine grid spacing to accurately trace the rays in the finite-difference eikonal approximation and to adequately resolve model features. Another method to improve confidence along boundaries is to incorporate information from vertical radar profiles (Knoll and Clement, 1999) and geophysical logging.

The different ray tracing routines in the inversions account for the different inverted velocity models. Boundaries are sharper and velocity changes are more distinct in the curved ray model. The ray coverage in the curved ray method shows that more rays are concentrated along

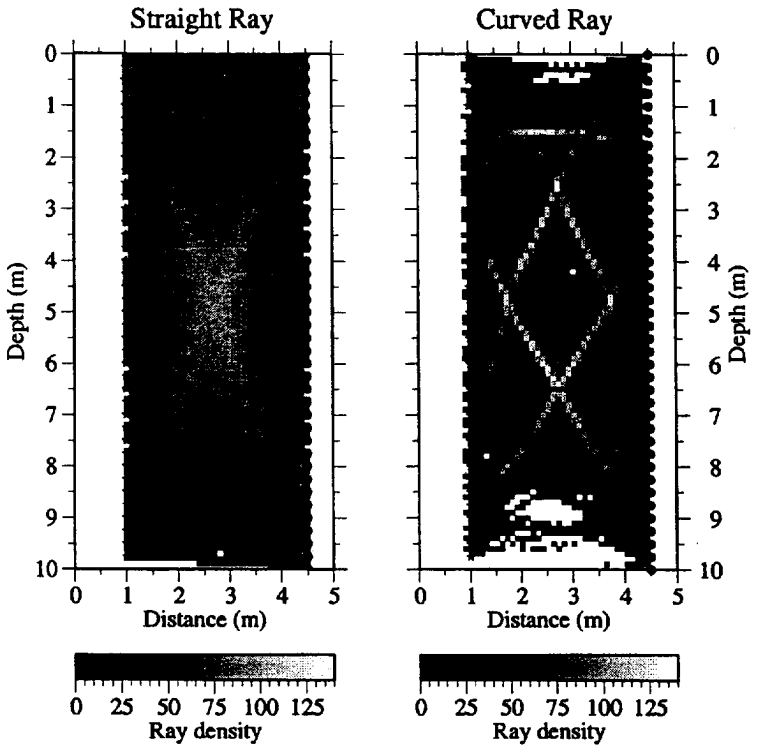

Figure 2. The ray coverage of the straight ray and the curved ray inversion. The grayscale indicates the changes in ray density. White areas are where rays do not sufficiently sample the model.

the boundaries in the model, especially along large velocity contrasts and high velocity zones. The curved rays more accurately model the refraction at the velocity boundaries since, by definition, the straight rays can not bend.

Constrained Inversion: Fixed Velocity Values

A variety of different types of constraints can be used in our effort to improve the resolution and accuracy of tomographic inversions. One type of constraint is to force specific velocity values on the inverse solution, such as specific layer properties. Tweeton (1988) has shown the value of including layer constraints in the inverse procedure. We ran a straight ray simulation, shown in Figure 3, to demonstrate this point. Constraining the upper 2 meters to be laterally constant produces a model that more sharply defines the water table boundary. The transition zone from the high velocity upper layer to the slower layer beneath is more sharply defined both vertically and horizontally. Moreover, the layering beneath the water table is more clearly defined as are the velocity changes in the two heterogeneous velocity layers. This relatively simple assumption, constant lateral velocity in the vadose zone, greatly improves the model reconstruction.

Constrained Inversion: Regularization

We also investigated the use of different types of regularization as constraints for the curved ray inverse procedure. We inverted the noise-free data using a flatness (first difference) constraint and a smoothness (second difference) constraint (Aldridge and Oldenburg, 1993). The flatness constraint seeks to find the model that does not contain velocity changes. In other words,

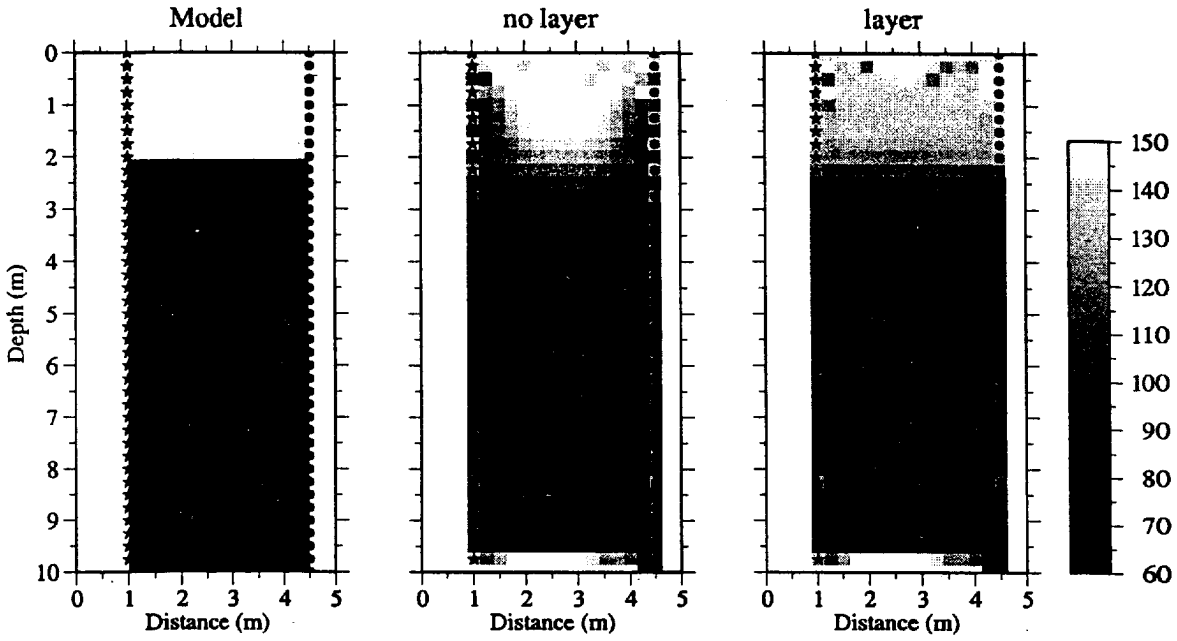

Figure 3. Effects of constraining upper layers to imitate the vadose zone. The center figure is inverted with smoothing only. In the right figure, the upper 2 m are constrained to have a laterally constant velocity. The grayscale indicates the velocity in m/μs. Note that the layering in the right figure is sharper and that the lateral velocity changes are more apparent and their velocity values contrast more.

we want a solution with as little change as possible. The smoothness constraint seeks to minimize the gradient of the velocity change in the designated direction, that is, we want a solution that has small changes in velocity gradient.

Figure 4 shows the results of the two different constraints on the curved ray inversion. The velocity variation is greater horizontally in the smoothness model than in the flatness model. This variation reflects the nature of the constraint; the smoothness constraint limits velocity gradient changes whereas the flatness constraint limits velocity changes. The ray coverage is similar between the two different models. Again, the similarity between the models indicates that the inversion is adequately modeling the data and that the choice of regularization constraint is not critical, at least for this earth model.

Effect of Grid Size

One decision that must be made in parameterizing a tomography problem is the size of the modeling grid cells. We used the straight ray algorithm to explore this issue. First, we inverted the data on a 0.5 m grid. In figure 5, we compare this result to the model using a 0.1 m cell size. The 0.5 m model contains larger amplitude velocity variations that are more sharply defined. Although the larger grid spacing better replicates the velocity variations, the model contains unreasonable velocity fluctuations, especially at the edges.

Importance of Starting Model

Another important parameter for curved ray tomographic inversions is the starting model for the nonlinear inversion. The inversion process traces rays through the starting model, then alters the model to reduce the misfit error. A danger in this iterative method is that the routine

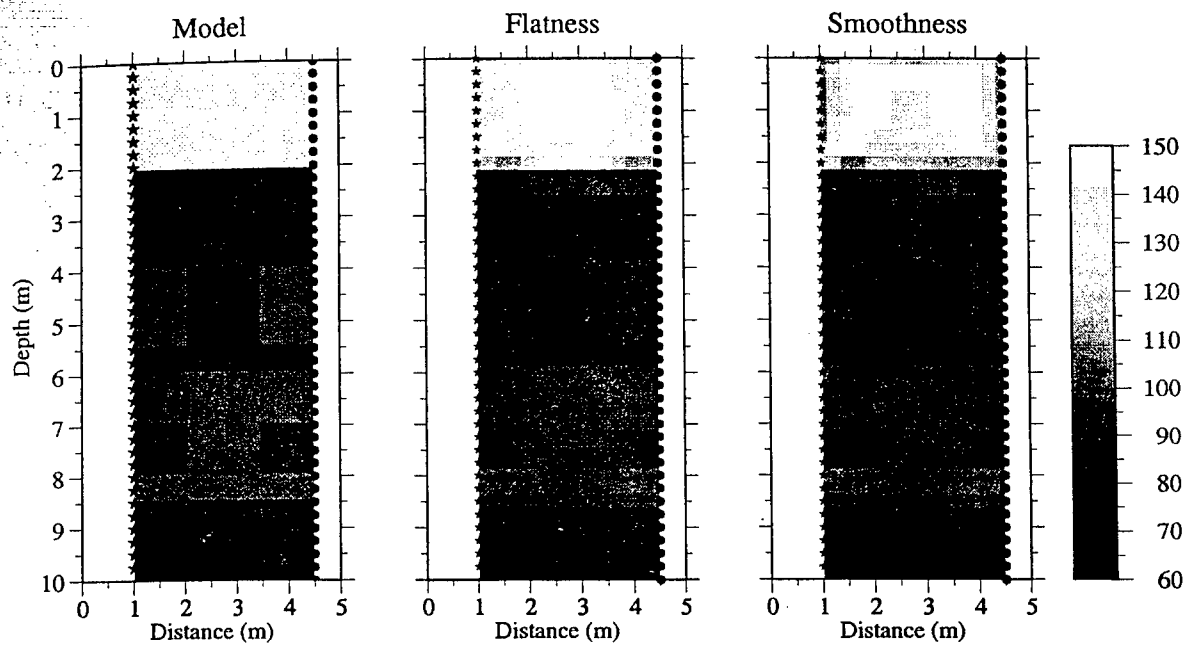

Figure 4. The tomogram in the center was computed with a flatness constraint. The tomogram on the right was computed with a smoothness constraint. The grayscale indicates the velocity in m/μs. The flatness constraint is the first derivative and the smoothness constraint is the second derivative. White regions indicate velocities greater than 0.150 m/μs.

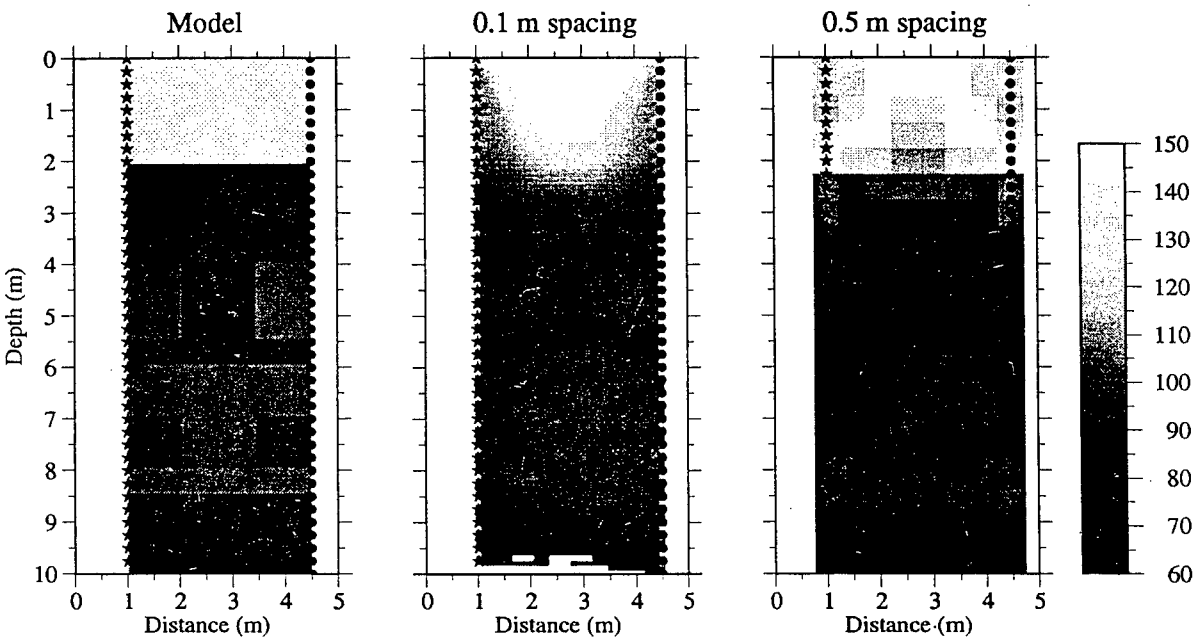

Figure 5. Comparing the effects of grid size in the model. The figure in the center was computed using 0.1 m grid spacing. The right figure has a grid spacing of 0.5 m. The grayscale indicates the velocity in m/μs. The white regions in the upper 2 m represent velocities greater than 0.150 m/μs. The white zone at the bottom of the center figure indicates a lack of ray coverage.

finds a local minimum, not the global minimum solution. To test that the solution is near the global minimum of the objective function, we inverted the data using several different starting models consisting of a homogeneous medium with a single velocity. We used velocities of 0.05, 0.09 and 0.20 m/ns to cover the range of realistic velocities for ground penetrating radar studies. The resulting tomograms are essentially the same, suggesting that the solution is close to the global minimum.

Effect of Noise

To investigate the effect of noise, we generated and then inverted two data sets, the first with no noise and the second with noise. We also added random noise to each travel time to simulate noisy data. The noise ranged from -0.5 to 0.5 ns. The results for the curved ray inversion are shown in Figure 6. Both methods model the noisy data about as well as they did the noise free data. The inversion statistics are very similar to the noise-free statistics, except that the RMS error values are larger, not an unexpected result. The level of noise that we added is realistic for borehole radar data (Saintenoy and Scales, personal communication).

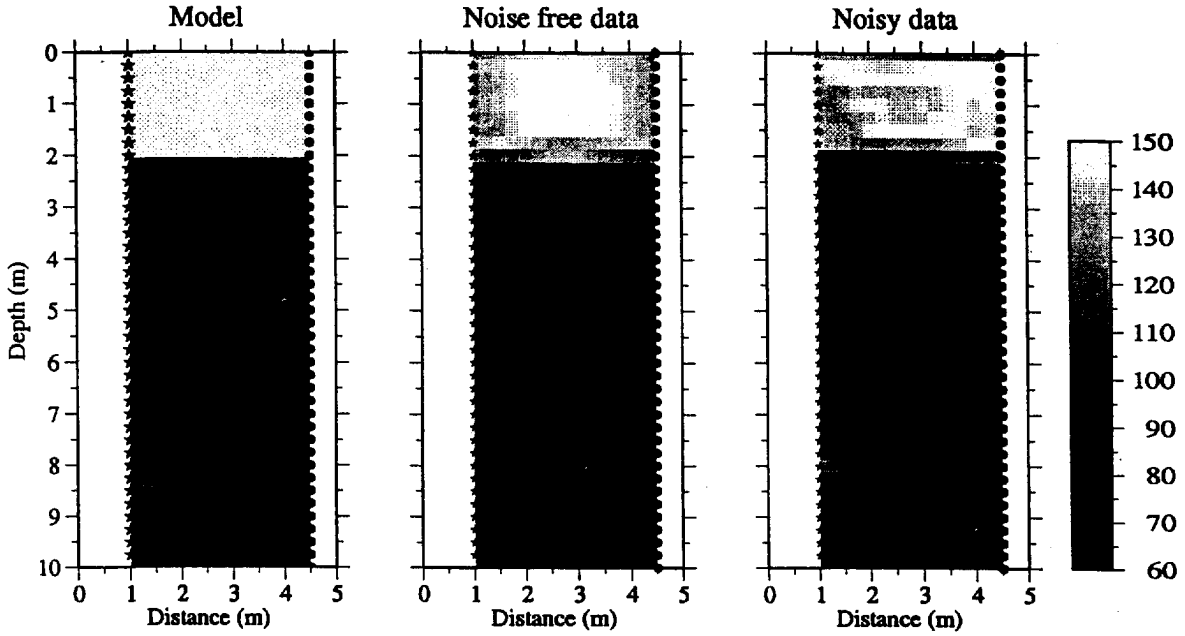

Figure 6. Comparison of inverting noise-free and noisy data. The two models were inverted with the curved ray algorithm with identical parameters. The grayscale corresponds to velocities in m/μs. Similar features are reconstructed in both figures. The noisy data has a larger variance in error misfit.

Effect of Ray Coverage

Finally, we study the effects of limited ray coverage on the model. The full data set has rays that encompass angles between -70° and 70°. In figure 7, we compare the full data set with data whose angular coverage is windowed to those rays between -40° and 40° and another set between -10° and 10°. The wider angular coverage better resolves the lateral horizontal velocity changes as well as the layer boundaries. As the angular coverage narrows, the lateral resolution decreases. In the -10° to 10° case, the model consists of horizontal layers with no apparent lateral

changes. With near surface tomography acquisition, wide angular coverages are limited by the distance the energy can propagate, not by the geometry of the experiment.

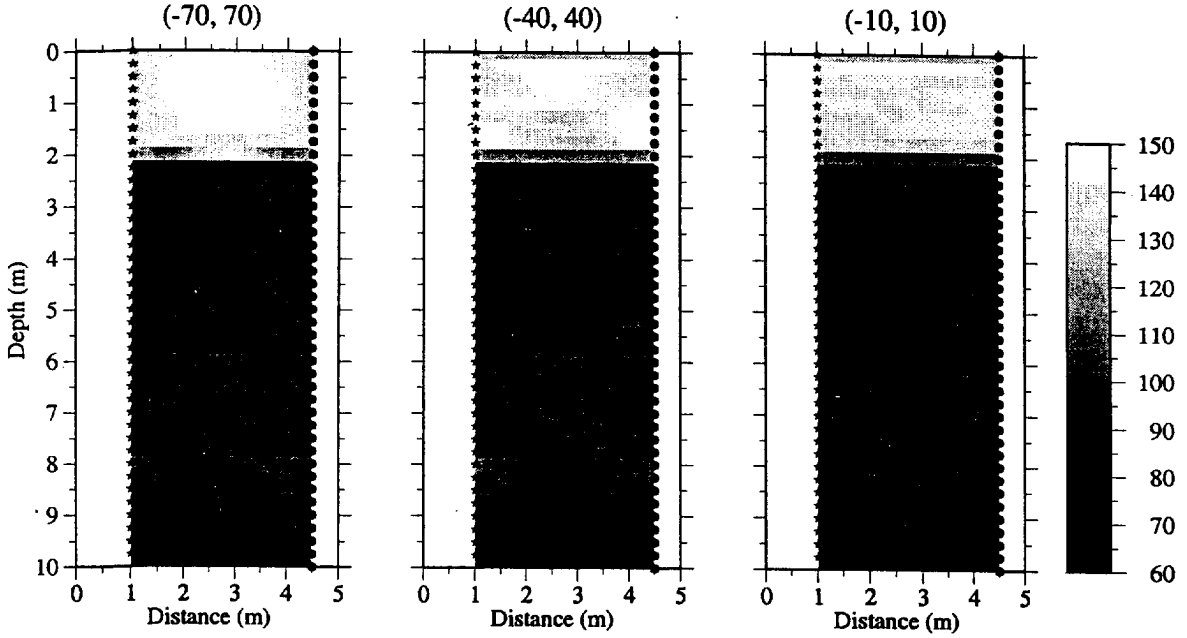

Figure 7. Effects of limited ray coverage. The full data set is used to compute the tomogram on the left. The angular coverage is between -70° to 70° from the horizontal. The tomogram in the center is computed with a limited aperture window with rays traveling between -40° and 40°, and the right tomogram has a window of -10° to 10°. The gray-scale indicates the velocity in m/μs.

SUMMARY

We have presented a synthetic modeling study to examine some of the issues that effect tomographic inversion of crosshole radar data. We looked at the effects of the forward model, the type of model constraints, the grid size, and the starting model. These factors are controlled by the inversion routines. We also examined the effect of noise in the data and ray coverage through the model. These effects are controlled by the field acquisition, and once the data has been collected, we can not change these factors.

The greatest effect on the inversion results is the choice of the forward model. The curved ray method better imaged the vertical and horizontal velocity changes. Another important effect on the inversion is the structure imposed on the solution. Inversions with some prior information about the structure of the sampled medium were better able to reconstruct the heterogeneities in the medium. Both curved and straight ray methods benefited from this type of information.

AKNOWLEDGMENTS

We thank Daryl Tweeton, Dave Aldridge, and Tom Clemo for helpful discussions clarifying inverse theory and tomography for us. This project is supported by U. S. Army Research Office grants DAAH04-96-1-0318 (URISP) and DAAG55-98-1-0277 (DEPSCoR). Contribution no. 0105 of the Center for Geophysical Investigation of the Shallow Subsurface at Boise State University.

REFERENCES

Aldridge, D. F. and Oldenburg, D. W., 1993, Two-dimensional tomographic inversion with finite-difference traveltimes, Journal of Seismic Exploration, 2, 257-274.

Barrash, W., Clemo, T., and Knoll, M. D., 1999, Boise Hydrogeophysical Research Site (BHRS): Objectives, design, initial geostatistical results, SAGEEP'99, 389-398.

Clement, W. P., Knoll, M. D., Liberty, L. M., Donaldson, P. R., Michaels, P., Barrash, W., and Pelton, J. R., 1999, Geophysical surveys across the Boise Hydrogeophysical Research Site to determine geophysical parameters of a shallow, alluvial aquifer, SAGEEP'99, 399-408.

Knoll, M. D., and Clement, W. P., 1999, Vertical radar profiling to determine dielectric constant, water content and porosity values at well locations, SAGEEP'99, 821-830.

Menke, W., 1989, Geophysical Data Analysis: Discrete Inverse Theory, Academic Press, Inc., 289 p.

Paige, C., and Saunders, M., 1982, LSQR: An algorithm for sparse linear equations and sparse least squares, Association of Computational Mathematics, Transactions on Mathematical Software, 8, 43-71.

Peterson, J. E. Jr.,Paulsson, B. N. P., and McEvilly, T. V., 1985, Applications of algebraic reconstruction techniques to crosshole seismic data, Geophysics, 50, 1566-1580.

Peterson, J. E., Jr., Majer, E. L., and Knoll, M. D., 1999, Hydrogeological property estimation using tomographic data at the Boise Hydrogeophysical Research Site, SAGEEP'99, 629-638.

Snieder, R., and Trampert, J., 1999, Inverse Problems in Geophysics, Samizdat Press, 72 p.

Tweeton, D. R., 1988, A tomographic computer program with constraints to improve reconstructions for monitoring in situ mining leachate, U. S. Bureau of Mines Report of Investigations, RI-9159, 70 p.

Vidale, J. E., 1990, Finite-difference calculation of travel times in three dimensions, Geophysics, 55, 521-526.